Eur. Phys. J. C 49, 347–353 (2007)
DOI 10.1140/epjc/s10052-006-0055-z

THE EUROPEAN PHYSICAL JOURNAL C

Regular Article – Theoretical Physics

Space-time evolution of hadronization

A. Accardi[a]

Department of Physics and Astronomy, Iowa State University, Ames, IA 50011, USA

Received: 31 July 2006 /
Published online: 6 December 2006 –

Abstract. Beside its intrinsic interest for the insights it can give into color confinement, knowledge of the space-time evolution of hadronization is very important for correctly interpreting jet-quenching data in heavy-ion collisions and extracting the properties of the produced medium. On the experimental side, the cleanest environment to study the space-time evolution of hadronization is semi-inclusive deeply inelastic scattering on nuclear targets. On the theoretical side, two frameworks are presently competing to explain the observed attenuation of hadron production: quark energy loss (with hadron formation outside the nucleus) and nuclear absorption (with hadronization starting inside the nucleus). I will discuss recent observables and ideas which will help to distinguish these two mechanisms and to measure the time scales of the hadronization process.

PACS. 25.30.-c; 25.75.-q; 24.85.+p; 13.87.Fh

1 Introduction

One of the most striking experimental discoveries in the heavy-ion program at the relativistic heavy-ion collider (RHIC) has been the suppression of large transverse momentum hadron production in nucleus–nucleus $(A+A)$ collisions compared to proton–proton $(p+p)$ collisions [1–4]. The observable of interest is the ratio of the hadron transverse momentum (p_{T}) spectrum in $A+B$ collisions in a given centrality class (c.cl.), normalized to binary scaled $p+p$ collisions by the inverse thickness function T_{AB} and finally divided by the $p+p$ spectrum:

$$R_{AB} = \frac{1}{T_{AB}(\text{c.cl.})} \frac{\mathrm{d}N^{A+B\to h+X}}{\mathrm{d}p_{\mathrm{T}}^2\,\mathrm{d}y}(\text{c.cl.}) \Bigg/ \frac{\mathrm{d}\sigma^{p+p\to h+X}}{\mathrm{d}p_{\mathrm{T}}^2\,\mathrm{d}y}\,. \tag{1}$$

In the absence of nuclear effects, one would expect $R_{AB} = 1$. By comparing the measured $R_{\mathrm{AuAu}} \approx 0.2$ in Au + Au collisions to the mild deformation of p_{T} spectra observed in deuteron–gold (d+ Au) collisions, one concludes that the large suppression of R_{AuAu} is due to the hot and dense medium produced in an Au + Au collision, also called "hot nuclear matter"; see Fig. 1. This measurement is one of the keys to the claimed discovery of the quark–gluon plasma (QGP) at RHIC [5].

The suppression of hadron production in $A+A$ collisions has been successfully described in terms of parton energy loss due to medium-induced gluon bremsstrahlung, allowing for so-called "jet tomography" studies of the QGP [6,7]. However, this success has recently been questioned. Gluon radiation off heavy quarks is expected on theoretical grounds to be suppressed at small angles compared to light quarks, implying a smaller suppression for D and B mesons than for π mesons [8]. However, the measured suppression of single non-photonic electrons at RHIC [9,10], which are the decay product of B and D mesons, is of similar magnitude for pions contrary to theoretical expectations [11,12]. The common assumption of neglecting elastic parton energy loss in R_{AA} computations has been recently reexamined [13], but the effect seems insufficient to explain the data, at least within conventional schemes for treating the running coupling constant [14]. A further assumption that needs to be tested and will be addressed in this paper is that the quark which fragments into the observed hadron traverses the whole medium and hadronizes well outside it. If untrue, in-medium interactions and screening of the hadronizing system would need to be accounted for.

Hadron suppression has also been observed in fixed target deep inelastic lepton–nucleus scattering (nDIS). In this case, the medium which induces the attenuation is the target nucleus itself, also called "cold nuclear matter"; see Fig. 1. Experimental data are usually presented in terms of the "multiplicity ratio" [15–20]

$$R_M^h(z_h) = \frac{1}{N_A^{\mathrm{DIS}}} \frac{\mathrm{d}N_A^h(z_h)}{\mathrm{d}z_h} \Bigg/ \frac{1}{N_D^{\mathrm{DIS}}} \frac{\mathrm{d}N_D^h(z_h)}{\mathrm{d}z_h}\,, \tag{2}$$

i.e., the single hadron multiplicity on a target of mass number A normalized to the multiplicity on a deuteron target

[a] e-mail: aaccardi@mail-cunuke.phys.columbia.edu

Based on a talk given at "Hot Quarks 2006", Villa Simius, Sardinia, Italy, May 15–20, 2006, and at "Future Prospect in QCD at High Energy", BNL, Upton, NY, July 17–22, 2006

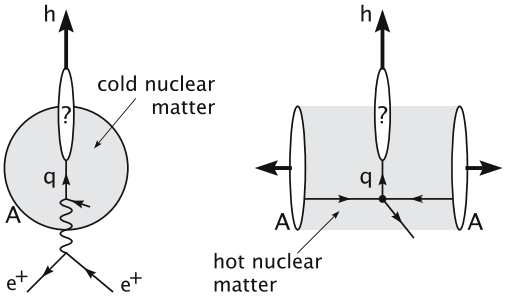

Fig. 1. *Left*: Lepton–nucleus scattering. The hadronizing quark travels through the target nucleus. *Right*: Nucleus–nucleus scattering. The hadronizing parton travels through the medium produced in the collisions. *Bold faced arrows* show the direction of motion of the colliding nuclei and the observed hadron

as a function of the hadron's fractional energy $z_h = E_h/\nu$, where ν is the virtual photon energy. The ratios in the numerator and denominator cancel to a large extent initial state effects like the modifications of parton distribution functions due to shadowing and EMC effects, exposing the nuclear modifications of the fragmentation process: if we assume factorization formulae to be valid, we have at leading order $R_M \approx D_h^A/D_h^D$, i.e., the ratio of the fragmentation functions (FF) in the nucleus A and in the deuteron. If no nuclear effects modify the fragmentation process we would expect $R_M \approx 1$. In fact, what is experimentally observed is hadron suppression in the $z_h = 0.2$–1 and $\nu = 2$–$20\,\mathrm{GeV}$ range at HERMES [16–18], and in the $\nu = 20$–$200\,\mathrm{GeV}$ at the EMC experiment [15]. The flavor dependence of the multiplicity ratio has also been measured [17, 18], showing suppression for pions, kaons and antiprotons. Protons are enhanced at $z_h \lesssim 0.4$ and suppressed above it: this is a "proton anomaly" analogous to the "baryon anomaly" observed in $p+A$ and $A+A$ collisions [1–4, 21, 22]. Both the quenching and the enhancement increase with A. Data binned in ν and in the photon virtuality Q^2 are also available from HERMES. Very high-statistics measurements will be available in the near future from the CLAS experiment at Jefferson Labs [19, 20], with some preliminary results having already been presented [23].

The cleanest environment to address nuclear modifications of hadron production is nuclear DIS: it allows one to experimentally control many kinematic variables; the nuclear medium (i.e., the nucleus itself) is well known; the multiplicity in the final state is low, allowing for precise measurements. Moreover, the nucleons act as femtometer-scale detectors of the hadronizing quark, allowing one to experimentally study its space-time evolution into the observed hadron. Hadron suppression at HERMES and CLAS is of direct relevance to RHIC physics. In both cases the hadronizing quark has to traverse a length of (hot or cold) nuclear matter of the size of a nuclear radius; see Fig. 1. Moreover, in the HERMES experiment $\nu \approx 2$–$25\,\mathrm{GeV}$ and $z_h \approx 0.2$–1, so that hadrons are observed over an energy range $E_h = z_h\nu = 2$–$20\,\mathrm{GeV}$. (measurements at CLAS with $E_{\mathrm{beam}} = 5.11\,\mathrm{GeV}$ will likewise explore the $E_h = 2$–$10\,\mathrm{GeV}$ range). For midrapidity hadron production in $A+A$ collisions at RHIC $E_h \approx p_{\mathrm{T}} \approx 2$–$20\,\mathrm{GeV}$, roughly equal to the hadron energy range at HERMES.

Information about parton propagation in cold nuclear matter is needed as an input for the interpretation of data in $A+A$ collisions. In this case one wants to use hadron suppression as a tool to extract the properties of the hot QGP created in the collision. To this purpose we need to develop well calibrated computational tools to relate the magnitude of hadron suppression to properties of the QGP like its density and temperature. Assuming long-lived partons, hadron suppression at RHIC would be attributed to parton energy loss, leading to a medium temperature of $T \approx 400\,\mathrm{MeV}$ [7], in excess of the critical temperature $T_{\mathrm{c}} \approx 170\,\mathrm{MeV}$ for the QGP phase transition. If, on the contrary, hadronization started on the nuclear radius scale or before it, in-medium interactions should also be accounted for, leading to a different, presumably lower T. Precise knowledge of parton propagation and hadronization mechanisms obtained from nDIS data is essential for testing and calibrating our theoretical tools, and to determine the properties of the QGP produced at RHIC.

2 Formation time estimates

The key quantity we need to investigate is the hadronization time scale. Since hadronization is a non-perturbative process, one has to resort to phenomenological models to describe it [24–31]. However, a few features are expected on general grounds. Due to color confinement, the struck quark must neutralize its color at some stage, say by picking up an antiquark from the vacuum or the surrounding medium. I call this color neutral $q\bar{q}$ pair a "prehadron" h_*, and the time for its formation the "prehadron formation time" t_* (some authors prefer to call it the "production" time). This is a relevant time scale since gluon bremsstrahlung off the struck quark stops after color neutralization; moreover, the prehadron quickly develops a cross section of the order of the hadronic one, leading to its nuclear absorption. Subsequently, the prehadron wave function collapses on the observed hadron h wave function, and the corresponding time is called the "hadron formation time" t_h. A final caveat: it is difficult to rigorously define the concept of formation time in field theory, so that in the following discussions it is used as a working tool.

2.1 Long formation time: energy loss models

The average hadron formation time $\langle t_h \rangle$ can be considered as the time for the struck partons to build up its color field and to develop the hadronic wave function [32]. In the hadron rest frame this time is related to the hadron radius, and in the laboratory frame it is boosted to

$$\langle t_h \rangle \propto R_h \frac{E_h}{m_h} = R_h \frac{z\nu}{m_h}\,. \tag{3}$$

For a 10 GeV pion at HERMES, we have $\langle t_h \rangle \approx 50\,\mathrm{fm} \gg R_A$. Note also that the scale for hadron formation is set

by $\kappa_h = m_h/R_h \approx 0.2\,\mathrm{GeV/fm}$. This estimate is used in energy loss models [24–26] assuming that hadronization starts outside the medium with a decreased parton energy due to multiple parton scatterings and induced gluon bremsstrahlung. These models are fairly successful in describing R_M at HERMES; see Fig. 2.

More in detail, [24] computes parton rescatterings and gluon radiation in pQCD including Feynman diagrams up to twist 4. Fragmentation of both the struck quark and the radiated gluon is included. The modification of the FF depends on one parameter, the strength of the parton–parton correlations in the nucleus. The modified FF so obtained can be modeled to a good accuracy by shifting z_h in the leading-twist fragmentation function:

$$\tilde{D}(z_h) \longrightarrow \frac{1}{1-\Delta z_h} D\Big(\frac{z_h}{1-\Delta z_h}\Big)\,, \tag{4}$$

where $\Delta z_h = \Delta E_q/\nu$ is the quark's fractional energy loss, and $\Delta E_q \approx 0.6\langle z_g\rangle$, with $\langle z_g\rangle$ the average fractional energy carried away by the radiated gluon.

In [25, 26] the parton energy loss is treated in the BDMS formalism [33], which takes into account medium-induced multiple soft gluon emission and fluctuations in the energy loss. Modified FF are computed as the average of the z_h-shifted FF in (4):

$$\tilde{D}_f^h(z_h) = \int_0^{(1-z)} \mathrm{d}\Delta z\, \mathcal{P}(\Delta z; \hat{q}, L_q) \frac{1}{1-\Delta z} D_f^h\left(\frac{z_h}{1-\Delta z}\right).$$

The "quenching weight" $\mathcal{P}(\Delta z)$ is the probability distribution of a fractional energy loss $\Delta z = \Delta E_q/\nu$ [33, 34], and L_q the quark's in-medium path length. The medium is characterized by the transport coefficient $\hat{q}$, which measures the average momentum transfer per unit path length from the medium to the parton. When also taking into account a realistic medium geometry and finite medium size corrections to the quenching weight, the model [35] can well describe HERMES data; see Fig. 2.

2.2 Short formation time: nuclear absorption models

A successful non-perturbative model of hadronization is the Lund string model [36]. The confined color field stretching from the struck quark to the rest of the nucleus is modeled as a string of tension $\kappa_{\mathrm{str}} \approx 1\,\mathrm{GeV/fm}$. Prehadron formation is identified with the $q\bar{q}$ pair production which breaks the string in smaller pieces [27]. Hadrons are formed when a quark and an antiquark at the endpoint of a string fragment meet. Average formation times can be analytically computed [27–29]:

$$\langle t_*\rangle = f(z_h)(1-z_h)\frac{z_h\nu}{\kappa_{\mathrm{str}}} \tag{5}$$

$$\langle t_h\rangle = \langle t_*\rangle + \frac{z_h\nu}{\kappa_{\mathrm{str}}}\,. \tag{6}$$

The factor $z_h\nu$ can be understood as a Lorentz boost factor. The $(1-z_h)$ factor is due to energy conservation: a high-z_h hadron carries away an energy $z_h\nu$; the string remainder has a small energy $\epsilon = (1-z_h)\nu$ and cannot stretch farther than $L = \epsilon/\kappa_{\mathrm{str}}$. Thus the string breaking must occur on a time scale proportional to $1-z_h$. The function $f(z_h)$ is only a small deformation of $\langle t_*\rangle$. At HERMES $\langle t_*\rangle \approx 4\,\mathrm{fm} < R_A$ and $\langle t_h\rangle \approx 6$–$10\,\mathrm{fm} \gtrsim R_A$. The hadron is typically formed at the periphery or outside the nucleus so that its interaction with the medium is negligible. However, the prehadron is formed well inside and can start interacting with the nucleus. The nuclear absorption model of [29] can successfully explain R_M measurements at HERMES in terms of prehadron–nucleon inelastic scatterings with the above formation times estimate; see Fig. 2. The prehadron–nucleon inelastic cross section is $\sigma_*(\nu) = 0.35\sigma_h(\nu)$, proportional to the experimental hadron–nucleon cross section σ_h. The proportionality factor is fitted to π^+ production data on a Kr target [17]. The prehadron survival probability S_* is computed in terms of transport equations. Neglecting hadron

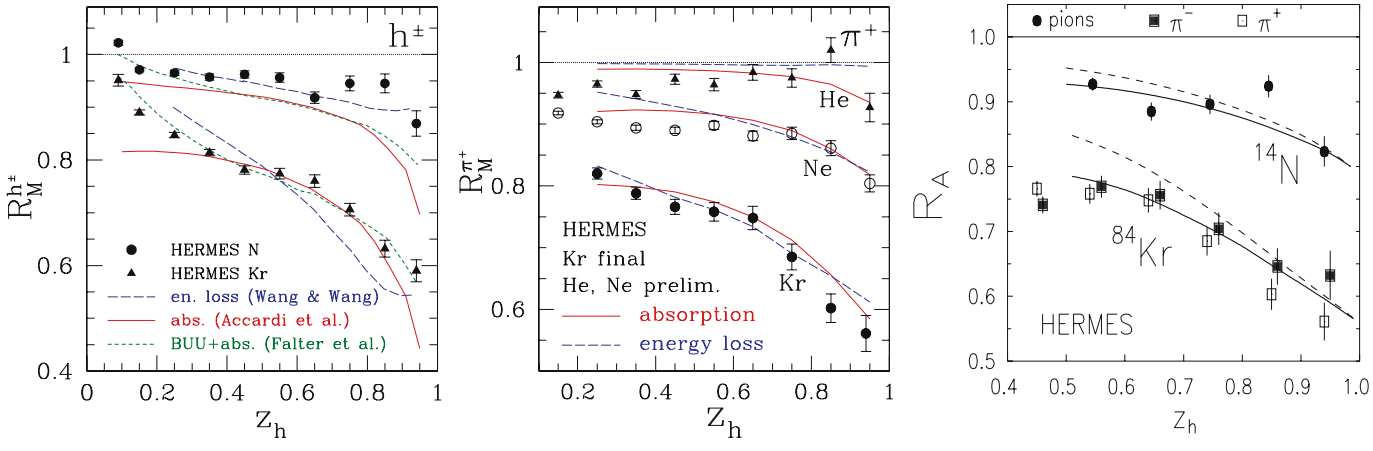

Fig. 2. *Left*: Multiplicity ratio for $h^\pm$ at HERMES [17] compared to the energy loss model of [24] and the absorption models of [29, 31]. *Center*: pure absorption model [29, 35] (*solid*) and energy loss model [25, 26, 35] (*dashed*). *Right*: Color dipole model [30] (*dashed*: absorption only, *solid*: absorption and induced energy loss). Data are from [16–18]

absorption,

$$S_* = \int \mathrm{d}^2b\,\mathrm{d}y\rho_A(b,y) \times \int_y^\infty \mathrm{d}x \frac{\mathrm{e}^{-\frac{x-y}{\langle t_*\rangle}}}{\langle t_*\rangle} \mathrm{e}^{-\sigma_* \int_x^\infty \mathrm{d}sA\rho_A(b,s)} ,$$

where (b,y) is the γ^*–q interaction point, ρ_A is the nuclear density, and one can recognize exponential probability distributions for prehadron and hadron formation.

In [30] the formation of a leading hadron ($z_h \gtrsim 0.5$) is described in a pQCD inspired model. The struck quark radiates a gluon according to the Bethe–Heitler radiation spectrum. The gluon then splits into a $q\bar{q}$ pair, and the $\bar{q}$ recombines with the struck q to form the leading prehadron. Medium interaction and evolution of the prehadron into the observed hadron is computed in a path-integral formalism for dipole propagation. The prehadron formation time is identified with the time at which the gluon becomes decoherent with the struck quark. The probability distribution in the prehadron formation time can be computed, and the average $\langle t_*\rangle$ is

$$\langle t_*\rangle \propto (1-z_h)\frac{z_h\nu}{Q^2} . \tag{7}$$

The scale is set by $\kappa_{\mathrm{dip}} = Q^2 \approx 10\,\mathrm{GeV/fm}$ at HERMES, and $\langle t_*\rangle \lesssim 5\,\mathrm{fm}$ at $z_h > 0.5$. This model can successfully describe leading hadron suppression; see Fig. 2, right.

In [31] a different space-time picture of hadronization is advocated. Prehadrons are formed at $t_* = 0$, and hadrons are formed at $t_h = (E_h/m_h)\tau_0$ with $\tau_0 = 0.5\,\mathrm{fm}$. The leading prehadron interacts with the medium with a reduced hadronic cross section. Subleading prehadrons do not interact with the medium until hadron formation. This picture is then embedded in a Monte Carlo transport model. A good description of HERMES data can be achieved; see Fig. 2.

3 Can we distinguish energy loss from hadron absorption?

Most of the difference in the time estimates quoted in the previous section lies in the different scale κ used. For example, $\kappa_h \approx 0.2\kappa_{\mathrm{str}}$ leads to the rather large $\langle t_h\rangle \approx 50\,\mathrm{fm}$ quoted in the energy loss model estimate instead of $\langle t_h\rangle \approx 10\,\mathrm{fm}$ quoted in the Lund model estimate. In the second case there would be no justification for neglecting the interactions of the forming hadron field with the nucleus. As the choice of the scale κ is a debatable and model-dependent matter [30, 37], it is very important to look for observables which are able to distinguish energy loss models and absorption models, or to directly detect in-medium hadronization effects.

3.1 Mass number dependence

In first approximation, one expects $1 - R_M^h \propto A^{2/3}$ in energy loss models because the average energy loss $\Delta E_q \propto \langle L_q^2\rangle \propto A^{2/3}$, due to the Landau–Pomeranchuk–Migdal interference in QCD [41]. On the other hand, in absorption models the survival probability is proportional to the amount of traversed matter, so that $1 - R_M^h \propto \langle L_A\rangle \propto A^{1/3}$. Therefore a simple analysis of the A-dependence of R_M^h should clearly signal which model is correct.

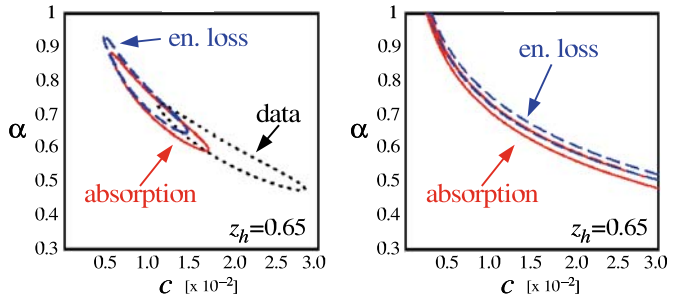

Fig. 3. *Left*: results of the $R_M = cA^\alpha$ fit for {He, N, Ne, Kr} at $z = 0.65$ (*solid*: absorption; *dashed*: energy loss; *dotted*: data [17]). *Right*: computations including only heavy nuclei {Kr, Sn, Xe, W, Au, Pb}

This argument fails for absorption models [29, 38]. If the prehadron were produced always at the γ^*–quark interaction point (i.e., $t_* = 0$) then $R_M = cA^{1/3}$ at all orders in $A^{1/3}$. However, if we allow for a non-zero $\langle t_*\rangle$, its dimension must be neutralized by the nuclear radius R_A, introducing extra powers of $A^{1/3}$. Quite generally, if the probability distribution for the prehadron formation length is finite at zero formation length, then $R_M^h \propto A^{2/3} + O(A)$, the same power found in energy loss models.

Then, we can study the *breaking* of the $A^{2/3}$ law. To this purpose, it was proposed in [29] to select a set of targets $\{A_1, A_2, \ldots, A_n\}$, fix the z bin, and perform a fit of the form $1 - R_M^h(z) = c(z)A^{\alpha(z)}$ with c and α free parameters. Results are presented in terms of 2σ confidence contours in the (c,α) plane. As shown in Fig. 3, left, energy loss [35] and absorption models [29, 35] are indistinguishable. The same holds true for all z bins. Experimental data are described by an A^α power law with $\alpha = 0.61 \pm 0.14$, compatible with $\alpha = 2/3$, but excluding $\alpha = 1/3$. Increasing the number of targets and the span in atomic number does not help in separating the two models, either, but clearly shows a non-negligible breaking of the $A^{2/3}$ law at $A \gtrsim 80$ [29, 35]; see Fig. 3, right.

3.2 Formation time scaling

In [39] I conjecture that R_M should not depend on z_h and ν separately but should depend on a combination of them:

$$R_M = R_M\left[\tau(z_h,\nu)\right] , \tag{8}$$

where the scaling variable τ is defined as

$$\tau = Cz_h^\lambda(1-z_h)\nu . \tag{9}$$

The scaling exponent λ is introduced as a way of approximating and summarizing the scaling behavior of experimental data and theoretical models. It can be obtained by

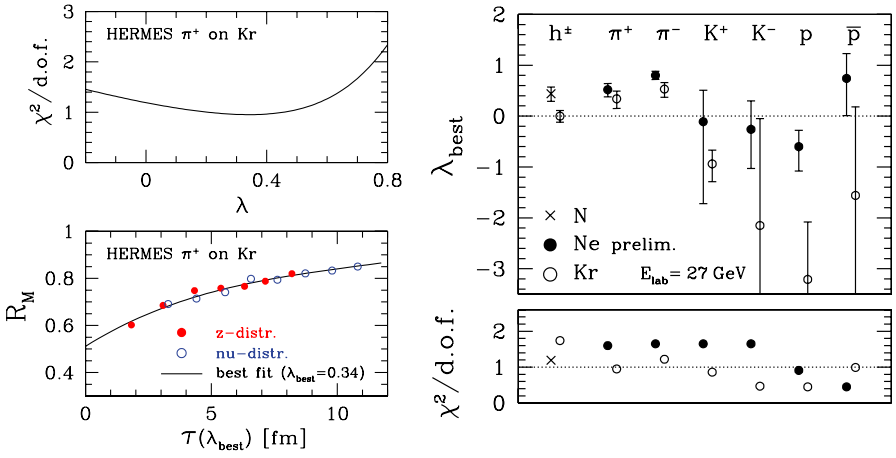

Fig. 4. *Left*: An example of the fit procedure described in Sect. 3.2 applied to HERMES data for π^+ production on a Kr target [17]. *Upper panel*: χ^2 as a function of λ. *Lower panel*: $R_M(\tau)$ with τ computed at $\lambda_{\rm best} = 0.34$. *Right*: The scaling exponent $\lambda_{\rm best}$ extracted from HERMES data on charged and identified hadrons at $E_{\rm lab} = 27$ GeV [16–18] (only statistical errors included in the fit). *Error bars* correspond to 1 standard deviation. The *bottom panel* shows the χ^2 per degree of freedom

a best fit analysis of data or theoretical computations. The proportionality constant C cannot be determined by the fit. A possible scaling of R_M with Q^2 is not considered in this analysis because of its model dependence, and because of the mild dependence of HERMES data on Q^2. As discussed below, the proposed functional form of τ, (9), is flexible enough to encompass both absorption models and energy loss models. The two classes of models are distinguished by the value of the scaling exponent: a positive $\lambda \gtrsim\!\!\!\not\; 0$ is characteristic of absorption models, while a negative $\lambda \lesssim 0$ is characteristic of energy loss models. Thus, the exponent λ extracted from experimental data can identify in the experimental data the leading mechanism for hadron suppression in nDIS.

The scaling of R_M is quite natural in the context of hadron absorption models [27–31]. Indeed, prehadron absorption depends on the in-medium prehadron path length, which depends solely on the prehadron formation time $\langle t_* \rangle$ as long as $\langle t_* \rangle \lesssim R_A$. As argued in Sect. 2, $\langle t_* \rangle \propto f(z_h)(1-z_h)z_h\nu$ which is well described by the proposed scaling variable τ with $\lambda > 0$. For instance, in the Lund model $\lambda \approx 0.7$.

In energy loss models [24–26, 35] the scaling is less obvious. For the purpose of discussing the scaling properties of R_M, we can consider the model of [25, 26, 35] and neglect finite medium size corrections and finite quark energy corrections. If we further neglect energy loss fluctuations, we can approximate $R_M \approx \widetilde{D}_A(z_h)/D(z_h)$ and obtain

$$R_M \approx \frac{1}{1-\langle\epsilon\rangle/\nu} D\left(\frac{z_h}{1-\langle\epsilon\rangle/\nu}\right) [D(z_h)]^{-1} \,,$$

where the average energy loss $\langle\epsilon\rangle = \int_0^{(1-z_h)\nu} \mathrm{d}\epsilon\epsilon\mathcal{P}(\epsilon) \,/\, \int_0^{(1-z_h)\nu} \mathrm{d}\epsilon\mathcal{P}(\epsilon) = f[(1-z_h)\nu]$ is a function of the energy $(1-z_h)\nu$ not carried away by the observed hadron. Next, we can approximate the FF using the parametrization of [40] at $Q^2 = 2\,\mathrm{GeV}^2$ and obtain

$$R_M \approx \frac{1}{\left(1-\frac{1}{\nu}f[(1-z_h)\nu]\right)^{\alpha+\beta+1}} \left(1-\frac{f[(1-z_h)\nu]}{(1-z_h)\nu}\right)^{\beta} .$$

This shows an approximate scaling with $(1-z_h)\nu$, which implies scaling of R_M with respect to τ with $\lambda \approx 0$. A similar argument holds for the model of [24]. When performing the scaling analysis of the full models one finds in general $\lambda \lesssim 0$ [39].

The HERMES experiment measures R_M binned in z_h and integrated over ν and Q^2 ("z_h distributions") or binned in ν and integrated over z_h and Q^2 ("ν distributions"). Equation (8) is fitted to the combined z_h and ν distributions, and the scaling exponent λ is determined by χ^2 minimization. An example of this procedure is illustrated in Fig. 4. Details can be found in [39].

The scaling exponents $\lambda_{\rm best}$ extracted from HERMES data at $E_{\rm lab} = 27$ GeV [16–18] for different hadron flavors produced on N, Ne and Kr targets are shown in Fig. 4. In all cases $\chi^2/\mathrm{d.o.f.} \lesssim 1.6$, which proves that R_M scales with τ. The central result of this analysis is that pion data exhibit a clear $\lambda_{\rm best} \approx 0.4 \gtrsim\!\!\!\not\; 0$. As discussed, this shows the dominance of the prehadron absorption mechanism as opposed to the energy loss mechanism, or in other words is a signal of in-medium prehadron formation, with formation times $\langle t_* \rangle \lesssim R_A$.

3.3 $p_{\rm T}$ broadening

The scaling analysis just described gives only indirect evidence for a short formation time and cannot measure its absolute scale. An observable which is more directly related to the prehadron formation time is the hadron's transverse momentum broadening in DIS on a nuclear target compared to a proton or deuteron target [30]. Indeed, when a hadron is observed in the final state, neither the quark nor the prehadron could have had inelastic scatterings. The prehadron–nucleon elastic cross section is very small compared to the quark cross section, so that the hadron's $p_{\rm T}$ broadening originates dominantly during parton propagation. As shown in [41, 42], the quark's momentum broadening $\Delta p_{\rm T}^2$ is proportional to the quark path length in the nucleus. If the prehadron formation time has the form (9) as argued in the last section, we obtain

$$\Delta p_{\rm T}^2 \propto \langle t_* \rangle \propto z_h^{\lambda}(1-z_h)\nu \,,$$

unless the distance of the quark production point from the surface of the nucleus is smaller than $\langle t_* \rangle$. Then we should

expect a decrease of Δp_{T}^2 with increasing z_h. This would be a clear and model-independent signal of in-medium prehadron formation: indeed, if the quark were traveling through the whole nucleus before prehadron formation Δp_{T}^2 would only depend on the nucleus size and not on z_h. A related observable is the z_h-dependence of the Cronin effect, which is likewise expected to decrease with increasing z_h [30].

The CLAS collaboration can perform multi-differential p_{T}-broadening measurements in all kinematic variables thanks to a very high beam luminosity. A few preliminary data from CLAS are already available [23]. The HERMES collaboration is also studying the p_{T} broadening at a larger beam energy but with a lower statistics. The scaling analysis proposed in the previous section will be useful to cross-check the results of these measurements.

4 Conclusions and perspectives

Use of hard processes to probe medium processes in $A+A$ collisions requires a detailed understanding of the hadronization process, which can be studied in lepton–nucleus scatterings. The scaling analysis [39] of pion attenuation at HERMES demonstrates for the first time a scaling of the hadron attenuation ratio R_M which is compatible with a short prehadron formation time of the order or smaller than the nuclear radius. Thus, it favors prehadron absorption as dominant mechanism for hadron suppression instead of gluon radiation off a struck quark. This conclusion will be soon checked by hadron p_{T}-broadening data.

Much more can be studied in lepton–nucleus scatterings.

(i) In the meson sector, the suppression of η mesons at RHIC, which is of similar magnitude than for π, seems to favor long-lived partons [43]. Measuring η and heavier meson attenuation at HERMES and CLAS will check the correctness of such interpretation.

(ii) Understanding the proton anomaly in nDIS will shed light on baryon transport in nuclear matter and on the baryon anomaly observed in $p+A$ and $A+A$ collisions. Measurements of Λ and other baryons at HERMES and CLAS will be needed in this respect.

(iii) Neither HERMES nor CLAS are able to study the hadronization of heavy quarks, because of limited luminosity and limited Bjorken's x coverage, respectively. The proposed Electron–Ion Collider [44] is well suited for such studies, thanks to its low-x coverage and high luminosity. Study of D and B meson suppression will settle the single electron puzzle at RHIC and will put interpretation of LHC data on a firmer ground. Study of "normal" J/ψ suppression will help in distinguishing competing mechanism and in building a precise baseline for measurements of the "anomalous" suppression in $A+A$ collisions.

Acknowledgements. I am very grateful to the organizers of this workshop for the financial support they offered me. I would like to thank V. Muccifora, D. Grünewald and H.J. Pirner for their collaboration on many results discussed in this work, and J.W. Qiu, P. Di Nezza, F. Arleo, C. Salgado, T. Falter and K. Gallmeister for valuable discussions. Figure 1 has been realized using JaxoDraw by D. Binosi and L. Theussl. This work is partially funded by the US Department of Energy grant DE-FG02-87ER40371.

References

1. BRAHMS Collaboration, I. Arsene et al., Nucl. Phys. A **757**, 1 (2005)
2. PHOBOS Collaboration, B.B. Back et al., Nucl. Phys. A **757**, 28 (2005)
3. STAR Collaboration, J. Adams et al., Nucl. Phys. A **757**, 102 (2005)
4. PHENIX Collaboration, K. Adcox et al., Nucl. Phys. A **757**, 184 (2005)
5. Brookhaven National Laboratory announcement, April 2005, http://www.bnl.gov/bnlweb/pubaf/pr/PR_display.asp?prID=05-38
6. M. Gyulassy, I. Vitev, X.N. Wang, B.W. Zhang, in Quark Gluon Plasma 3, ed. by R.C. Hwa, X.N. Wang (World Scientific, Singapore) [arXiv:nucl-th/0302077]
7. I. Vitev, J. Phys. G **30**, S791 (2004)
8. Y.L. Dokshitzer, D.E. Kharzeev, Phys. Lett. B **519**, 199 (2001)
9. STAR Collaboration, J. Bielcik, arXiv:nucl-ex/0511005, and these proceedings
10. PHENIX Collaboration, S.S. Adler et al., Phys. Rev. Lett. **96**, 032 301 (2006)
11. M. Djordjevic et al., Phys. Lett. B **632**, 81 (2006)
12. N. Armesto et al., Phys. Lett. B **637**, 362 (2006)
13. S. Wicks et al., arXiv:nucl-th/0512076
14. A. Peshier, arXiv:hep-ph/0605294, and these proceedings [arXiv:hep-ph/0607275]
15. EMC Collaboration, J. Ashman et al., Z. Phys. C **52**, 1 (1991)
16. HERMES Collaboration, A. Airapetian et al., Eur. Phys. J. C **20**, 479 (2001)
17. HERMES Collaboration, A. Airapetian et al., Phys. Lett. B **577**, 37 (2003)
18. HERMES Collaboration, G. Elbakian et al., Proceedings "DIS 2003", St. Petersburg, April 23–27, 2003, ed. by V.T. Kim, L.N. Lipatov, p. 597
19. CLAS Collaboration, B.A. Mecking et al., Nucl. Instrum. Methods A **503**, 513 (2003)
20. W.K. Brooks, Fizika B **13**, 321 (2004)
21. J.W. Cronin et al., Phys. Rev. D **11**, 3105 (1975)
22. D. Antreasyan et al., Phys. Rev. D **19**, 764 (1979)
23. W.K. Brooks, talk at Jefferson Laboratory Users Group Workshop, June 13, 2006
24. E. Wang, X.N. Wang, Phys. Rev. Lett. **89**, 162 301 (2002)
25. F. Arleo, Eur. Phys. J. C **30**, 213 (2003)
26. F. Arleo, JHEP **0211**, 044 (2002)
27. A. Bialas, M. Gyulassy, Nucl. Phys. B **291**, 793 (1987)
28. A. Accardi, V. Muccifora, H.J. Pirner, Nucl. Phys. A **720**, 131 (2003)
29. A. Accardi, D. Grunewald, V. Muccifora, H.J. Pirner, Nucl. Phys. A **761**, 67 (2005)

30. B.Z. Kopeliovich, J. Nemchik, E. Predazzi, A. Hayashigaki, Nucl. Phys. A **740**, 211 (2004)
31. T. Falter, W. Cassing, K. Gallmeister, U. Mosel, Phys. Rev. C **70**, 054 609 (2004)
32. Y.L. Dokshitzer, V.A. Khoze, A.H. Mueller, S.I. Troian, Basics of Perturbative QCD (Ed. Frontières, Gif-sur-Yvette, France, 1991)
33. R. Baier, Y.L. Dokshitzer, A.H. Mueller, D. Schiff, JHEP **0109**, 033 (2001)
34. C.A. Salgado, U.A. Wiedemann, Phys. Rev. D **68**, 014 008 (2003)
35. A. Accardi, arXiv:nucl-th/0510090
36. B. Andersson et al., Phys. Rep. **97**, 31 (1983)
37. X.N. Wang, Phys. Lett. B **579**, 299 (2004)
38. H.P. Blok, L. Lapikas, Phys. Rev. C **73**, 038 201 (2006)
39. A. Accardi, arXiv:nucl-th/0604041
40. B.A. Kniehl, G. Kramer, B. Potter, Nucl. Phys. B **582**, 514 (2000)
41. R. Baier et al., Nucl. Phys. B **484**, 265 (1997)
42. M.B. Johnson et al., Phys. Rev. C **63**, 035 203 (2001)
43. PHENIX Collaboration, S.S. Adler et al., Phys. Rev. Lett. **96**, 202 301 (2006)
44. A. Deshpande et al., Ann. Rev. Nucl. Part. Sci. **55**, 165 (2005)